

DOI: 10.1002/cmdc.200900452

Pyrrolidine Derivatives as Plasmepsin Inhibitors: Binding Mode Analysis Assisted by Molecular Dynamics Simulations of a Highly Flexible Protein

Torsten Luksch,^[a] Andreas Blum,^[a] Nina Klee,^[a] Wibke E. Diederich,^[a] Christoph A. Sotriffer,^[a, b] and Gerhard Klebe^{*[a]}

Plasmepsins II (EC number: 3.4.23.39) and IV (EC number: 3.4.23.B14) are aspartic proteases present in the food vacuole of the malaria parasite *Plasmodium falciparum* and are involved in host hemoglobin degradation. A series of pyrrolidine derivatives, originally synthesized as HIV-1 protease inhibitors, were tested for activity against plasmepsin (Plm). Inhibitors in the nanomolar range were discovered for the Plm II and IV isoforms. Detailed studies were carried out to identify putative binding modes that help to explain the underlying structure–activity relationships. Reasonable binding modes were generat-

ed for pyrrolidine-3,4-diester derivatives and a substituted 3,4-diaminopyrrolidine inhibitor by using a crystal structure of inhibitor-bound Plm II (PDB ID: 1LEE). Modeling studies indicated that the flap of available Plm crystal structures is not sufficiently opened to accommodate the 3,4-bis(aminomethylene)pyrrolidines. Molecular dynamics simulations were performed to analyze the flexibility of the protein in greater detail, leading to a binding mode hypothesis for the 3,4-bis(aminomethylene)pyrrolidines and providing further insight and general implications for the design of Plm II inhibitors.

Introduction

Malaria is one of the main infectious diseases in the world, with about one million fatalities per year.^[1] It is caused by parasites of the genus *Plasmodium*. The species that infect humans are *P. falciparum*, *P. malariae*, *P. ovalae*, and *P. vivax*. Of these species, *P. falciparum* causes the most life-threatening form of malaria. The organism is transmitted by the female *Anopheles* mosquito.^[1] General symptoms of the disease are fever, chills, nausea, and flu-like illness, which in severe cases lead to coma and death. Although there are several antimalarial drugs on the market, the increasing number of multi-drug-resistant parasite strains requires the development of novel therapeutic agents.^[2,3]

Plasmepsins have been described as promising targets for the discovery of antimalarials. They belong to the family of aspartic proteases and are involved in the initial steps of hemoglobin degradation, which is the main source of amino acids for the parasite.^[4,5] The catabolism of human hemoglobin takes place during the erythrocytic stage within the acidic food vacuole of the parasite. Although recent evidence has shown that *P. falciparum* can survive without vacuolar plasmepsins under culture,^[6] many plasmepsin (Plm) inhibitors are fatal to the parasite.^[7–10] There are four plasmepsins present in this lysosome-like organelle: Plm I,^[8,11] Plm II,^[4,12] Plm IV,^[13] and HAP (histo-aspartic protease).^[13] The redundant functional role of these enzymes in hemoglobin digestion has been demonstrated by Plm gene deletion. This suggests that more effective drugs may be obtained by simultaneously blocking multiple Plm isoforms.^[14,15]

Recently, a novel 3,4-bis(aminomethylene)pyrrolidine scaffold was designed and synthesized as a general aspartic protease inhibitor lead structure.^[16] The scaffold core was decorated

with side chains from other ligands known to be well suited to address the specificity pockets of the enzyme.^[17] K_i values in the low micromolar range were observed toward HIV-1 protease as well as cathepsin D. The crystal structure of this inhibitor in complex with HIV-1 protease was subsequently determined (PDB ID: 1XL2). In a second design cycle, 10 additional compounds were synthesized.^[18]

Although HIV-1 protease belongs to the retroviral proteases whereas Plms are aspartic proteases with a pepsin-like fold, various examples of inhibitors designed for HIV-1 protease also show strong inhibition of Plm II.^[19–21] The two proteins share sequence similarities that could be responsible for the similar inhibition profiles; in particular, they exhibit identical catalytic dyad and peptide recognition motifs.^[16] Furthermore, both aspartic proteases feature a common flap (two in HIV-1 protease) that is involved in ligand binding. The flaps close upon substrate accommodation, thereby excluding solvent from the inner catalytic cavity of the enzyme.^[22] Because our pyrrolidine derivatives were designed to address the family-wide features of aspartic proteases, we anticipated inhibition of the Plms as well.

[a] Dr. T. Luksch, Dr. A. Blum, N. Klee, Prof. Dr. W. E. Diederich, Prof. Dr. C. A. Sotriffer, Prof. Dr. G. Klebe
Philipps-Universität Marburg
Institut für Pharmazeutische Chemie
Marbacher Weg 6, 35032 Marburg (Germany)
Fax: (+49) 6421-28-28994
E-mail: Klebe@staff.uni-marburg.de

[b] Prof. Dr. C. A. Sotriffer
Current address: Universität Würzburg
Institut für Pharmazie und Lebensmittelchemie
Am Hubland, 97074 Würzburg (Germany)

To suggest reasonable binding modes, previously solved Plm II crystal structures were analyzed for their suitability to accommodate the pyrrolidine-type scaffold described herein. Because only limited structural information is available for the highly flexible Plms, molecular dynamics (MD) simulations were also performed and analyzed in detail.

Initial MD simulations for Plm II were performed in 2001.^[23] Within a short simulation time of 100 ps, residues that play an important role in hydrogen bonding to the inhibitor were identified. In the research group of Åqvist, several MD simulations of protein–ligand complexes were carried out in order to determine binding modes and to predict K_i values for compounds with various scaffolds such as dihydroxyethylenes, macrocyclic inhibitors, and allophenylnorstatine inhibitors.^[24–28] Recently, MD simulations were also used to obtain insight into the maturation process from pro-Plm II to Plm II^[29] and to derive guidelines for the design of selective Plm inhibitors.^[30] MD studies have further been used to assess the relative stability of putative ligand binding modes, as recently studied for the binding of halofantrine to Plm.^[31] All these studies indicate that Plm is a difficult and highly flexible target and that MD simulations are helpful and necessary to overcome the limited structural information available.

Results and Discussion

Enzyme inhibition

A total of 10 compounds were tested for activity against Plm II, Plm IV, and the human aspartic protease cathepsin D (Cat D). They can be divided into three molecule classes with different core structures (1, 2, and 3; Table 1). Compounds 1.1–1.7 belong to the first series of molecules containing a 3*S*,4*S*-pyrrolidinediol scaffold 1, which is symmetrically decorated, via esterification, with substituents of various size and polarity. The second compound class is composed of a 3*S*,4*S*-diaminopyrrolidine core 2 and is substituted with two benzyl and two benzoyl moieties. Compounds 3.1 and 3.2 are racemic mixtures of *trans*-3,4-bis(aminomethylene)pyrrolidines 3, both decorated with four side chains that presumably interact with the sub-pockets of different aspartic proteases (Table 1).

Well-diffracting crystals for HIV-1 protease in complex with a 3,4-bis(aminomethylene)pyrrolidine derivative were obtained.^[17] The crystals were grown in the presence of a racemic inhibitor mixture.^[17] Because the 3*R*,4*R*-bis(aminomethylene)pyrrolidine stereoisomer was found in the crystal structure (PDB ID: 1XL2), it was hypothesized that the *R,R* enantiomer binds more strongly than the *S,S* enantiomer. Encouraged by these results, a second compound series to inhibit HIV-1 protease was synthesized (compounds 1.1–1.7) by following an enantioselective synthetic route.^[18] To optimize key interactions toward the flap residues of HIV-1 protease, the scaffold was altered by decreasing the linker length. In addition, the number of appended side chains was limited to two. Compounds 1.1–1.7, originally synthesized for HIV-1 protease, were also tested against Plm II, Plm IV, and Cat D.

Table 1. Experimental inhibitory activities of the compounds studied.

Compd	Chemical Structure	Enzyme K_i [μM]		
		Plm II	Plm IV	Cat D
1				
1.1		51.2	168	> 1000
1.2		47.2	41.2	> 1000
1.3		11.4	7.4	53.4
1.4		19.0	53.8	> 1000
1.5		163	134	> 1000
1.6		1.0	0.8	0.5
1.7		0.10	0.09	0.37
2				
2		0.43	1.5	11.7
3				
3.1		0.63	0.35	0.67
3.2		0.50	0.18	0.37

While the 3,4-bis(aminomethylene)pyrrolidines 3.1 and 3.2 exhibited K_i values in the sub-micromolar range, the pyrrolidine-3,4-diester derivatives functionalized with two monocyclic

aromatic rings resulted only in single- and double-digit micromolar activities. For example, **1.3** showed a K_i value of 11 μM for Plm II, 7 μM for Plm IV, and 53 μM for Cat D.

Within the series of derivatives bearing **1** as the core element, compounds with isobutyl, neopentyl, and cyclohexyl moieties were the weakest binders to the Plms, with K_i values in the high double- and triple-digit micromolar range (**1.1**, **1.2**, and **1.5**). For Cat D, no inhibition was detected up to 1 mM. A gain in affinity was achieved by replacing the alkyl chains with monocyclic aromatic ring systems. With a K_i value of 11 μM toward Plm II, **1.3** is about fourfold more potent than **1.2** ($K_i = 47 \mu\text{M}$). Similar results were obtained for Plm IV (sixfold increase in affinity). The removal of one methylene unit (compound **1.4**) relative to **1.3** has almost no effect on the binding affinity to Plm II, whereas a sevenfold decrease was detected for Plm IV. The pyrrolidine-3,4-diester equipped with two 2-naphthyl moieties further increased the potency (compound **1.6**). The K_i value of **1.6** for Plm II is 1 μM , with slightly better K_i values for Plm IV and Cat D (0.8 and 0.5 μM , respectively). The most potent inhibitor in this series is **1.7**, with a K_i value of 100 nM for Plm II and 90 nM for Plm IV. It shows a 1600-fold greater binding affinity for Plm II than **1.5**, the weakest-binding inhibitor of all compounds measured.

The calculated ligand efficiency of **1.1** is 0.31 (in $\text{kcal mol}^{-1} \cdot [\text{no. of heavy atoms}]^{-1}$) for Plm II and 0.27 for Plm IV.^[32,33] These values are promising, as inhibitors with ligand efficiencies ~ 0.3 are considered efficient binders.^[34] The ligand efficiency for the largest compound **1.7** is 0.29 for both Plm II and IV, and is thus similar to **1.1**. This is remarkable, as it has been observed that ligand efficiency depends on ligand size, with smaller ligands having greater efficiencies, on average, than larger ligands.^[35] Based on the observation that the maximum observed ligand efficiency decreases for molecules with higher numbers of heavy atoms, Reynolds et al. introduced a new scoring scheme termed ligand "fit quality" that normalizes the ligand efficiency values: Most efficient binders in the data set were scaled to have a top score of 1.0 across a wide range of molecular sizes.^[35] The calculated ligand "fit quality" values of **1.7** for both Plms are 0.95, which indicates near-optimal ligand binding.

Replacing the ester functionalities with amide groups, and following subsequent decoration with four benzyl moieties, inhibi-

tor **2**, with K_i values of 430 nM for Plm II and 1.5 μM for Plm IV, was obtained. In comparison to the most potent compounds of series **1**, inhibitor **2** shows a decreased ligand efficiency (0.21 for Plm II and 0.19 for Plm IV), but reasonable ligand "fit quality" values of 0.84 for Plm II and 0.76 for Plm IV were still achieved. Fortunately, slight improvements in selectivity toward human cathepsin D were observed.

Docking studies

Currently, 15 *P. falciparum* Plm II-inhibitor complex crystal structures are available; these can be subdivided into three groups exhibiting different ligand binding modes.^[36] Pepstatin A and related ligands are tightly embraced by the protein (PDB IDs: 1SME, 1ME6, 1XDH, 1XE5, 1XE6, 1W6I, 1W6H, 1M43, and 2R9B). The hydroxy group of the statine moiety forms hydrogen bonds to the catalytic dyad (Figure 1a). A difference is only observed for the peptide-based ligand in a recently solved crystal structure (PDB ID: 2R9B), in which the hydrogen bonds to the catalytic dyad are mediated by a water molecule. Further key interactions are formed by two inhibitor amide oxygen atoms to the backbone nitrogen of V78 and to the side chain of S79. Both amino acids belong to a β -hairpin structure, known as a "flap", that closes with a virtually perpendicular orientation to the binding cleft. The flap is a flexible

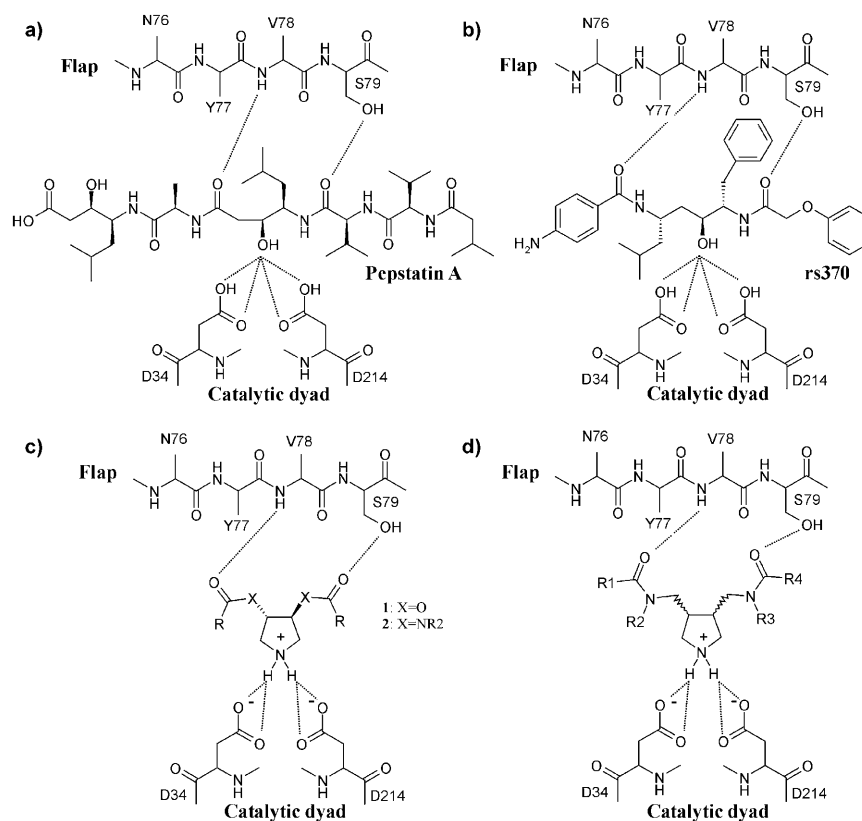


Figure 1. Hydrogen bonds of a) pepstatin A and b) rs370 in the active site of Plm II. c) Putative hydrogen bonds of 3S,4S-diesterpyrrolidine **1** and 3S,4S-diaminopyrrolidine **2** to Plm II. d) Putative hydrogen bonds of 3,4-bis(amino-methylene)pyrrolidine **3** to Plm II.

structural unit, present in all aspartic proteases, that interacts with substrates and inhibitors.^[37,38]

The second group of ligands found in co-crystal structures (PDB IDs: 1LEE, 1LF2, and 1LF3) comprises a hydroxypropylamine scaffold that forms a similar pattern of conserved hydrogen bonds to the catalytic aspartates and the flap residues V78 and S79^[39] as the pepstatin-A-like ligands (Figure 1 b). In these complexes, the binding cavity remains more open than in the pepstatin A complexes.^[40]

The third group of ligands present in co-crystal structures (PDB IDs: 2BJU, 2IGY, and 2IGX) induces significant differences in the protein conformation.^[41] The N-substituted piperidine scaffold interacts with the catalytic aspartates via an interstitial water molecule. Moreover, no interactions to the flap residues are observed. Instead, major changes in the flap region occur, and a new tunnel-shaped hydrophobic cavity opens up.

In the design of derivatives with **1**, **2**, and **3** as core structures, it was anticipated to directly address both the aspartate residues of the catalytic dyad and the flap residues (Figure 1 c,d). Therefore, the choice of Plm II in the open conformation and in the conformation found in the complex structure with pepstatin A was considered as a promising starting point for our considerations to generate appropriate binding modes.

A co-crystal structure of HIV-1 protease with a scaffold related to **3** is available (PDB ID: 1XL2). The central pyrrolidine moiety is found at the pivotal position between the two catalytic aspartate residues.^[17] The ring adopts an envelope conformation, and both ring substituents are found in an axial position. Experimental pK_a values for unsubstituted pyrrolidines suggest the central nitrogen atom of the ligand is protonated.^[42] Furthermore, pK_a calculations of a pyrrolidine derivative in complex with HIV-1 protease suggest that both catalytic aspartates of the HIV-1 protease should be deprotonated upon ligand binding.^[43] Recently, the crystal structure of **1.7** in complex with HIV-1 protease was determined (PDB ID: 3BC4).^[18] Although binding of the pyrrolidine nitrogen atom to the catalytic dyad was observed, no polar interactions with the flap region were detected due to an alternate protein conformation revealing an open flap. Based on these differences, only the structure in the closed-flap conformation (PDB ID: 1XL2) was considered for the generation of a putative binding mode for Plm II.

Taking the aforementioned findings as a prerequisite for our model generation, we tried to manually place the ligand core structures of **1–3** into different

conformers of Plm II found either in the complex with pepstatin A (PDB ID: 1SME) or in the more open complex structure (PDB ID: 1LEE). The pyrrolidine nitrogen atom was considered as protonated, whereas the catalytic dyad was considered to be fully deprotonated as suggested by pK_a model calculations on HIV-1 protease.^[43] The ligand functionalities assigned to interact with the flap region (Figure 1 c,d) were rotated toward the backbone nitrogen atom of V78 and to the side chain of S79.

For all three ligand series, hydrogen bonds could not be formed to the flap residues as found in the orientation observed in the closed Plm II conformer with bound pepstatin A (PDB ID: 1SME). However, manual placement of **1** and **2** into the binding pocket of the more open complex structure (PDB ID: 1LEE) could be achieved. In order to optimize these initial ligand geometries, an energy minimization was performed. During this minimization using the MOLOC MAB force field^[44] the protein was kept rigid, allowing full flexibility of the inhibitor. In all minimized complexes the pyrrolidine core position remains between the two catalytic aspartates, making short-distance hydrogen bonds to both carboxylate groups. Additional hydrogen bonds are formed to the flap residues V78 and S79 (Figure 2). The side chains of all energy-minimized inhibitors point toward the S2 and S2' pockets.

As described above, the activity of compounds **1.1–1.7** increases in the order: isobutyl < benzyl < 2-naphthyl < 1-naphthyl (Table 1). The modeled binding modes support these findings (Figure 2). S2 and S2' are spacious pockets that are not fully occupied by small side chains such as a 1-isobutyl substituent (Figure 2a). The larger benzyl moiety can form better hydrophobic interactions (Figure 2b). A further gain in affinity is observed for two 2-naphthyl substituents. The inhibi-

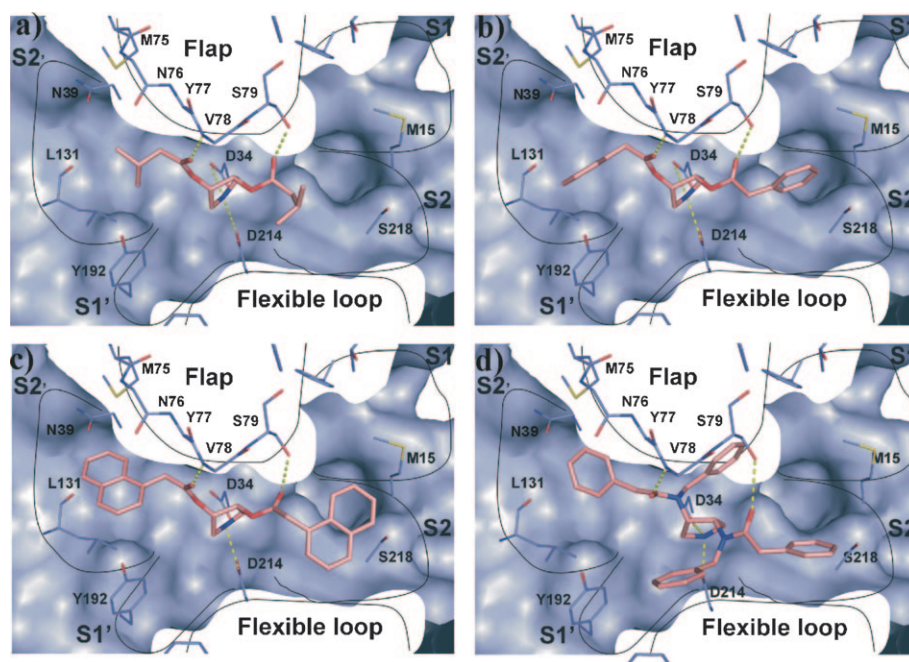


Figure 2. Modeled binding modes of compounds a) **1.1**, b) **1.3**, c) **1.7**, and d) **2** in the binding pocket of Plm II (PDB ID: 1LEE).

tor with two 1-naphthyl groups shows a tenfold improved affinity relative to the 2-naphthyl-substituted diester, with a K_i value of 100 nM for Plm II. This can be attributed to the more favorable burial of the ligand side chains in the S2 and S2' pockets (Figure 2c).

A similar binding mode can be proposed for **2** bearing the 3*S*,4*S*-diaminopyrrolidine scaffold: Both aspartates as well as the flap residues V78 and S79 are addressed by **2** (Figure 2d). The four side chains of this inhibitor are placed in the four sub-pockets (S1, S2, S1', and S2') forming hydrophobic interactions.

The compounds of series **1** and **2** were synthesized as pure enantiomers, exhibiting an *S,S* configuration at both stereogenic centers.^[18] The synthesis of **2** is outlined below in the Experimental Section. The derivatives of series **3** have been prepared and tested as racemic mixtures.^[17] Considering the crystal structure with HIV-1 protease, only the 3*R*,4*R* enantiomer was detected,^[17] which leads to the assumption that this enantiomer represents the more potent binder.

In analogy to the results observed for HIV-1 protease, improved binding of the *R,R* enantiomer of **3** is also anticipated for Plm II. Docking of these stereoisomers of **3.1** and **3.2** to the Plm II conformer (PDB ID: 1LEE) was attempted. However, no reasonable binding mode could be generated in which all interactions with the flap region and the catalytic dyad are present. Clearly, the lid of the flap would have to open further in order to allow hydrogen bond formation with the two aspartates and residues V78 and S79 simultaneously. Nevertheless, because potent binding is experimentally observed, the question arises whether Plm II can adapt to host **3.1** to **3.2** in an extended binding pocket. To gather insight into the dynamic properties of the enzyme, MD simulations were performed.

Molecular dynamics simulations

The available structural data indicate that Plm II is a highly flexible protein. For example, in the asymmetric unit of the Plm II-pepstatin A co-crystal structure (PDB ID: 1SME) two molecules are found that do not exhibit the same conformation, indicating intrinsic inter-domain flexibility.^[38] Furthermore, a comparison of uncomplexed Plm II (PDB ID: 1LF4) with Plm II in complex with EH58 (PDB ID: 1LF3) reveals movements of residues in the binding pocket to accommodate bulky groups of the inhibitor or to form hydrogen bonds.^[40]

Until now, only three distinct binding modes for the different inhibitor classes have been discovered. Structural studies indicate, however, that Plm II allows significant conformational flexibility and could possibly adapt in a way to accommodate derivatives **3.1** and **3.2** with the extended pyrrolidine core structure.

To further sample the conformational space of the protein and to explore its adaptive properties, a multi-nanosecond MD simulation was performed. We recently reported MD simulations of uncomplexed Plm II. The obtained results helped to rationalize unexpected binding in two examples.^[36,45] Encouraged by these results, we extended the simulation time from

1 ns to 10 ns and closely monitored further conformational transitions along the trajectory.

In the remainder, we focus exclusively on the binding site region as the area of highest interest in the context of structure-based drug design, particularly with respect to the issue of flexibility. A total of 32 residues were selected as part of the binding pocket. Mobility in this region is quantitatively analyzed by a mutual comparison of individual frames along the trajectory in terms of a 2D RMSD plot. For this purpose, 500 snapshots were extracted at regular 20 ps intervals along the entire 10 ns trajectory. It is immediately apparent that three main conformational sub-states can be distinguished (Figure 3).

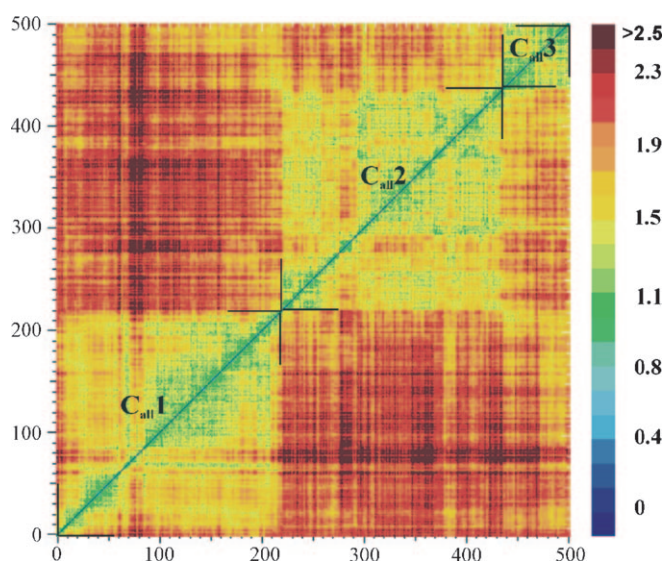


Figure 3. 2D RMSD plot using snapshots extracted every 20 ps. The mutual RMSD between two snapshots is represented by the color code displayed at right. All values are given in Å. For the RMSD measurements, all side chain atoms were included.

The first conformational sub-state is sampled for 4.3 ns at the beginning of the trajectory ("conformation_{all} 1", C_{all}1). The second conformational family C_{all}2 is then maintained for about 4.4 ns before a transition to C_{all}3 occurs, which remains for the following 1.2 ns. Conformations within the same sub-state show RMSD values mostly < 1.4 Å, while conformations of different sub-states show RMSD values of up to 2.3 Å.

To detect the molecular changes giving rise to this conformational flip, we further divided the binding pocket into individual sub-pockets (S1, S2, S1', and S2') and generated 2D RMSD plots for each of them (Figure 4).

The S2 pocket (T35, S215, T217, S218, A219, T221, and I290) remains nearly unchanged and represents essentially only one conformation along the entire trajectory (Figure 4a). The RMSDs of these residues are comparatively low, with movements of 1.3 Å on average.

Similar behavior is assumed for the S1' pocket (Q194, N210, I212, L292, F294, and I300), but here the overall RMSDs among the snapshots are significantly higher (Figure 4b) and reach

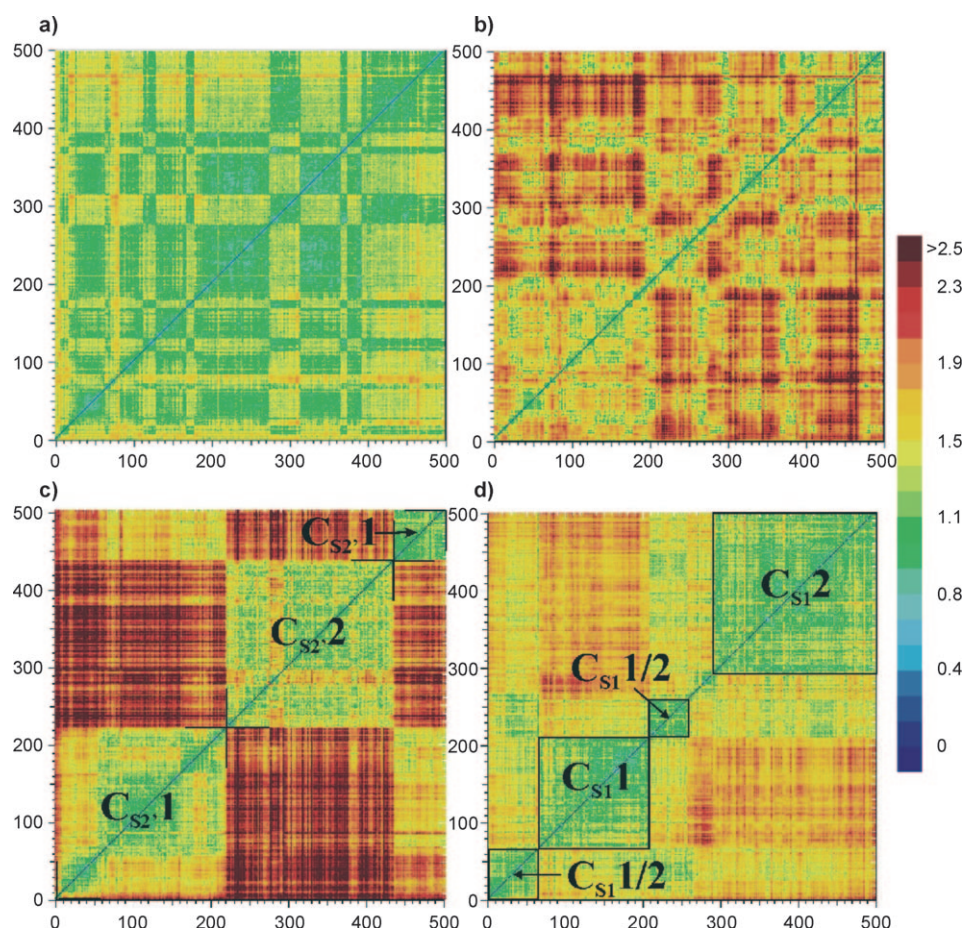


Figure 4. 2D RMSD plot using snapshots extracted every 20 ps. The mutual RMSD between two snapshots is represented by a relative color code shown at right. All values are given in Å. Only residues of the S2 pocket are considered in a), of the S1' pocket in b), of the S2' pocket in c), and of the S1 pocket in d). For the RMSD measurements, all side chain atoms were included.

values of up to 4.0 Å (red areas). The residues responsible for this fluctuation are F294 (average RMSD with respect to the reference crystal structure: 2.8 ± 0.8 Å) and L292 (2.4 ± 0.6 Å), whereas all other residues in this pocket show less pronounced changes. A maximal RMSD value of 5.8 Å (with respect to the reference crystal structure) was detected for F294. These results are consistent with the observations by Ersmark et al.^[20,24] describing a slight expansion of the S1' pocket by side chain rotations of F294 and L292 necessary for the accommodation of bulky P1' groups.^[20,24]

Two major distinct states of the S2' pocket (G36–N39, M75–V78, L131–I133, and Y192) can be discerned from its 2D RMSD plot (Figure 4c). The distribution of clusters highly resembles the findings for the entire binding pocket, indicating that the overall parent conformations ($C_{all}1$, $C_{all}2$, and $C_{all}3$) are mainly determined by changes in the S2' pocket. Interestingly, a sudden and clear-cut transition from the first ($C_{S2}1$) to the second state ($C_{S2}2$) is observed after 4.3 ns. The second conformational family is maintained for about 4.4 ns ($C_{S2}2$), before a new one-step transition back to geometries closely related to $C_{S2}1$ occurs. A comparison of the 2D RMSD plots (Figure 4a–d) indicates that a transition of the conformational states within

the S2' pocket does not directly affect transitions of the other sub-pockets. Therefore, the movements of the particular sub-pockets appear to be rather independent of each other.

The amino acids N76–V78 are known to interact with P2' substituents. Their mobility is pronounced, as they are involved in closing and opening of the flap. These movements are of particular interest with respect to the search of a putative binding-competent conformer to accommodate ligands with scaffold 3. This is discussed in greater detail in the next section. Residues in this pocket close to the catalytic dyad (G36–A38) show little structural mobility, whereas large deviations are observed for N39, M75, I133, and Y192 (Table 2). Side chain movements for N39 ($N\chi_1$ and $N\chi_2$) are especially pronounced, which could be important for ligand binding. Upon a 180° rotation of the terminal amide function, hydrogen bond acceptor and donor functionalities are mutually interchanged.^[36] Similarly, no particular state is predominantly popu-

Table 2. RMSD for residues of the S2' pocket.^[a]

Residue	Average RMSD [Å]	Standard Deviation [Å]	Maximum RMSD [Å]	Minimum RMSD [Å]
G36	1.5	0.3	3.1	0.5
S37	1.5	0.4	2.7	0.3
A38	1.3	0.3	2.5	0.4
N39	2.0	0.3	3.4	0.3
M75	2.2	0.3	3.5	1.1
I133	3.6	1.3	8.1	0.4
Y192	2.2	0.6	5.2	0.3

[a] RMSD for residues of the S2' pocket with respect to the reference crystal structure, averaged over the entire trajectory, with standard deviation as well as maximum and minimum values; measurements were carried out including all side chain atoms.

lated for Y192. This residue fluctuates between different states with a maximal deviation of 5.2 Å. Therefore, the hydroxy group of Y192 could possibly be addressed by ligands to form hydrogen bonds as observed for all pepstatin-A-like ligands.

An extensive flexibility of the S2' pocket has also been described by Ersmark et al. mainly based on side chain move-

ments of M75.^[24] Analysis of the $M\chi_2$ angle along the trajectory resulted in similar observations (Figure 5). The χ_2 angle exhibits a high standard deviation of 45° from the mean value of 118° .

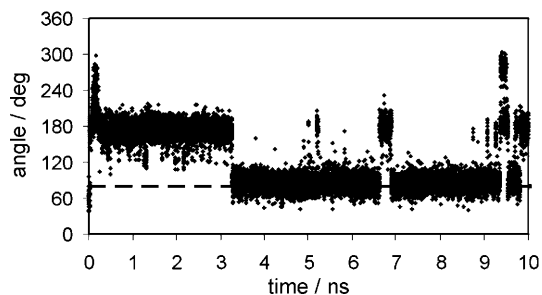


Figure 5. Fluctuation of the $M\chi_2$ angle in M75 in the MD simulation of Plm II, with the corresponding value from the crystal structure shown as reference.

In addition to the conformation found in the crystal structure, one particular conformation is highly populated and seems to be energetically favorable. Similar observations are made for the χ_3 angle: a high standard deviation of 65° from the average value of 54° caused by two highly populated alternative conformations. In the crystal structure, the M75 side chain extends into the $S2'$ pocket. Upon rotation it oscillates toward the interior of the enzyme, thereby opening and closing the pocket.

However, despite this dynamic behavior of M75, residue I133 plays the key role. The RMSD plot (Figure 6) shows an ele-

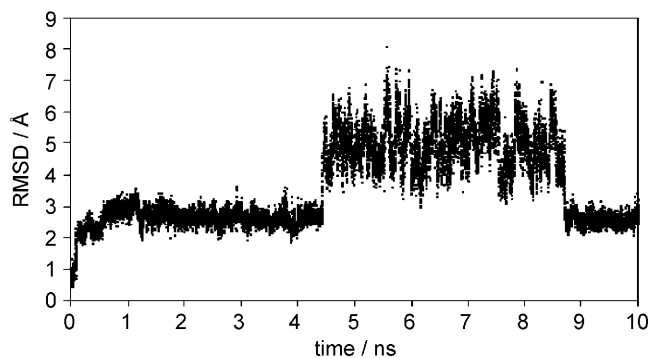


Figure 6. All-atom RMSD of I133 from the reference crystal structure as a function of simulation time.

vated average RMSD value of 3.6 \AA with a high standard deviation (1.3 \AA) and a maximal deviation of 8.1 \AA . During the first 4.3 ns the average RMSD is $< 3 \text{ \AA}$ with low standard deviations. For the next 4.4 ns the RMSD increases to 5 \AA with high standard deviations, and returns back to 3 \AA during the last 1.3 ns. These time steps are identical to those observed in the overall 2D RMSD plot (Figure 3), indicating that this residue is responsible for the distinct conformational states in the $S2'$ pocket.

RMSD fluctuations should not be over-interpreted and must be complemented by qualitative visual inspections. A comparison of frames extracted from each cluster provides insight into

the conformational states sampled during the simulations (Figure 7). Based on the 2D RMSD plot for the $S2'$ pocket (Figure 4c), four MD-generated snapshots are compared, showing all residues of this pocket (G36–N39, M75–V78, L131–I133, and Y192). The snapshots are representatives from three different clusters: The first frame (1_{S2}) belongs to the cluster in the lower left of Figure 4c ($C_{S2}1$), the second and third frames (2_{S2} and 3_{S2}) originate from the center cluster ($C_{S2}2$), and the fourth frame (4_{S2}) is extracted from the cluster in the upper right ($C_{S2}1$).

The superposition of the first (1_{S2}) and second frame (2_{S2}) shows that, with the exception of I133, no significant conformational variations are given (Figure 7a). The mobility of I133 is not restricted to the side chain level, but includes backbone movement as well. The C^α atom is shifted by 4.2 \AA , and the side chain rotates outward from the $S2'$ pocket. As shown by a comparison of the surface representations of the two frames, I133 swings out and opens up a wider pocket in 2_{S2} (Figure 7b,c), enabling the accommodation of ligands with more bulky groups. The potent inhibitor **1.7** with a bulky 1-naphthyl substituent predicted to point into the $S2'$ pocket supports this finding. The transition from frame 2_{S2} to frame 4_{S2} is illustrated in Figure 7d. As in Figure 7a, the $S2'$ flanking residues roughly remain at their positions, except for I133. A superposition of 1_{S2} , a representative of cluster 1 ($C_{S2}1$, Figure 4c lower left) with 4_{S2} from cluster 3 ($C_{S2}1$, Figure 4c upper right) clearly shows that I133 adopts the same orientation in both cases, and indeed both frames represent the same conformational state (Figure 7e). Figure 7f shows that residues found in two snapshots extracted from the same cluster occur with closely related geometry (both frames belong to cluster $C_{S2}2$, Figure 4c).

As Ersmark et al. collected data only up to 2 ns, whereas in our simulation the first major conformational change occurs after 4.3 ns, the results are in agreement that as long as the sub-pockets remain in one conformational state, no significant displacement of the backbone portion is observed during the MD simulations.^[24]

The 2D RMSD plot for the $S1$ pocket (M15, I32, S79, F111, T114, F120, and I123) is shown in Figure 4d. In contrast to the 2D RMSD plots for the $S2'$ pocket and the entire binding site, the borderlines between two conformational states are less pronounced. The first occurring conformational family is maintained for 1.4 ns ($C_{S1}2$). After the appearance of the cluster $C_{S1}1$ for 2.8 ns, a conformational flip back to $C_{S1}2$ is observed for 1 ns. This is followed by a transition to $C_{S1}2$. This conformational state is retained for 4 ns. While the clusters $C_{S1}1$ and $C_{S1}2$ are distinct from each other, $C_{S1}2$ exhibits similarities to both $C_{S1}1$ and $C_{S1}2$ and is therefore considered as an intermediate conformational state. While F120, I32, and I123 appear rather rigid during the MD simulation, residues M15, S79, F111, and T114 show elevated flexibility (Table 3).

In most of the available crystal structures the hydroxy group of S79 in the flap region is involved in the formation of crucial hydrogen bonds to a bound ligand. Residue S79 experiences an average RMSD of 2.4 \AA with a standard deviation of 0.7 \AA , resulting in maximal values of $\sim 5 \text{ \AA}$. Similarly, the orientation

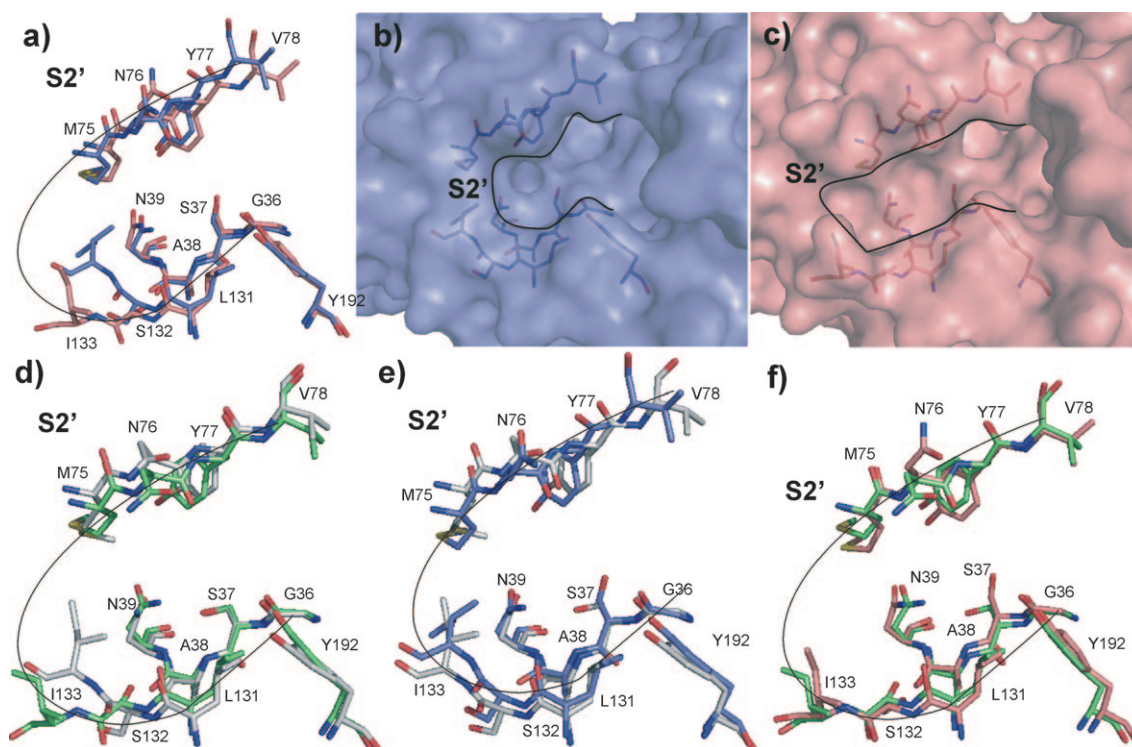


Figure 7. Fluctuation of the S2' pocket. a) Superposition of the frames 1_{S2'} (blue) and 2_{S2'} (salmon) extracted from cluster C_{S2'1} and C_{S2'2} (Figure 4c). b) Surface representation of 1_{S2'} in blue. c) Surface representation of 2_{S2'} in salmon. d) Superposition of the frames 3_{S2'} (green) and 4_{S2'} (gray). e) Superposition of the frames 1_{S2'} (blue) and 4_{S2'} (gray). f) Superposition of the frames 2_{S2'} (salmon) and 3_{S2'} (green).

Residue	Average RMSD [Å]	Standard Deviation [Å]	Maximum RMSD [Å]	Minimum RMSD [Å]
M15	2.1	0.5	3.8	0.7
I32	1.1	0.2	2.2	0.7
S79	2.4	0.7	5.1	0.6
F111	1.7	0.6	3.8	0.3
T114	1.9	0.5	4.3	0.4
F120	1.0	0.3	2.4	0.2
I123	0.8	0.2	2.1	0.2

[a] RMSD for residues of the S1 pocket with respect to the reference crystal structure, averaged over the entire trajectory, with standard deviation as well as maximum and minimum values; measurements were carried out including all side chain atoms.

of the hydroxy group, described by the $S\chi_1$ angle, is involved in the pronounced flexibility. This observation might be important for finding a putative binding mode for the 3,4-bis(amino-methylene)pyrrolidine derivatives. No highly populated preferred state is observed for T114, indicating that this residue fluctuates over multiple states.

M15 and F111 are responsible for the occurrence of distinct states of the S1 pocket, as illustrated in Figure 8a–c. Discarding these two crucial residues for the generation of the 2D RMSD plot results in one preferred conformer of the S1 pocket described by the remaining residues (Figure 8a). Discarding either one of the flexible residues from the analysis produces

2D RMSD plots with different distinct states exhibiting clear borderlines (Figure 8b,c).

The flexibility of M15 was recently addressed by us.^[45] Fluctuations in the $M\chi_1$ and $M\chi_2$ angles result in an expansion of the S1 pocket. As a consequence, the pocket is capable of accommodating norstatine derivatives with large hydrophobic side chains.

To analyze the conformations of F111 in greater detail, representative frames extracted from the C_{S1_M1} and C_{S1_M2} cluster (Figure 8b) were selected and visually inspected. The superposition of both frames shows that movements of S79, M15, and F111 cause the main structural differences in the S1 pocket (Figure 8d). Primarily responsible for the occurrence of the distinct sub-states in Figure 8b is the rotation around the $F\chi_2$ angle of F111.

Putative binding mode generation for 3,4-bis(amino-methylene)pyrrolidines

As discussed above, a conformational opening of the flap is required to establish key interactions to the 3,4-bis(amino-methylene)pyrrolidines. The involved residues N76–S79 at the tip of the flap region indeed show pronounced flexibility during the simulations (Table 4).

The backbone atoms of the flap region move ~5 Å in total relative to the crystal structure. Snapshots along the trajectory that show shifts of ~2 Å should be suited to reasonably accommodate scaffold 3. Because this is well within the range of the observed average RMSDs, a MD-generated snapshot could

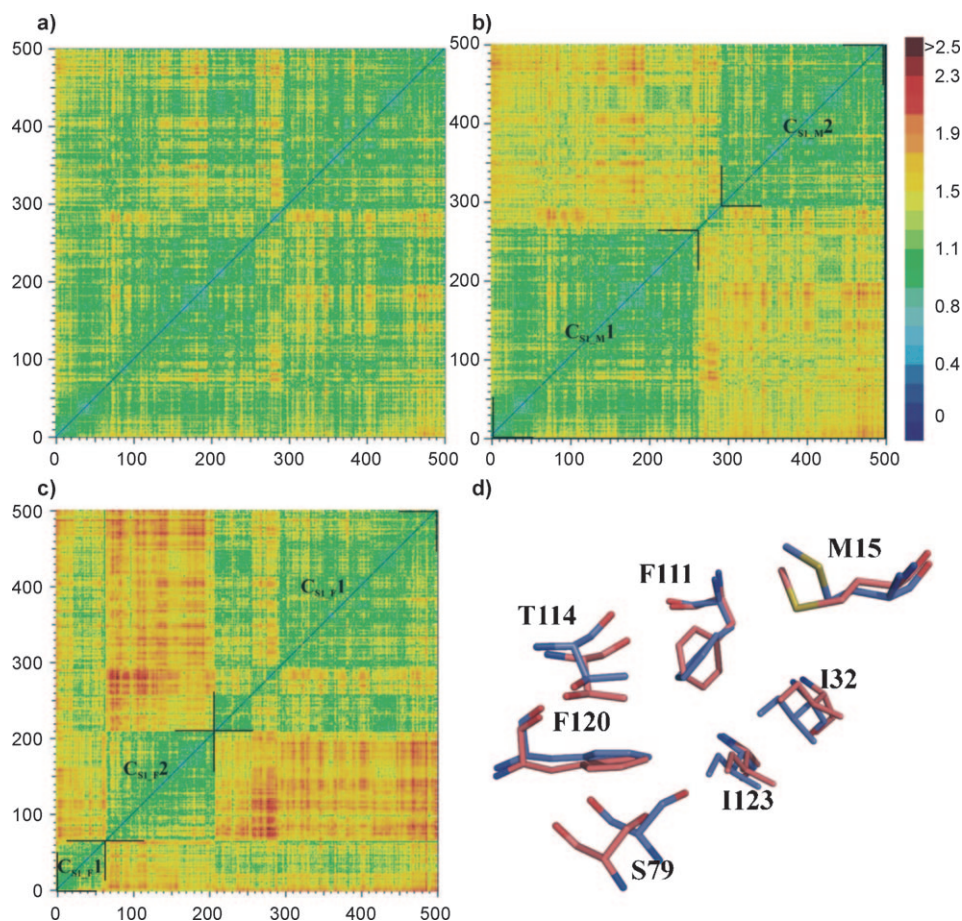


Figure 8. 2D RMSD plot considering residues of the S1 pocket discarding: a) M15 and F111, b) M15 only (two main conformational sub-states can be distinguished that originate from fluctuations of F111), and c) F111 only (the observed conformational sub-states originate from fluctuations of M15). d) A frame taken from the cluster C_{S1_M1} (red) is superimposed with a representative member from cluster C_{S1_M2} . The χ_2 angle of F111 remains nearly unchanged for the first 5 ns, but then shows a rotation of about 90° . This conformation is retained for the last 4 ns. S79 also shows elevated flexibility, but no preferentially populated state is observed, indicating that this residue fluctuates over multiple states. For the RMSD measurements, all side chain atoms were included.

be easily identified that fulfills the requirements in order to establish key interactions to **3**. Ligand **3.2** was manually placed between the catalytic aspartates of the selected snapshot, keeping the ring geometry as observed in the HIV-1 protease crystal structure (PDB ID: 1XL2; Figure 9). The amide oxygen atoms were rotated toward V78 and S79. The geometry was

Table 4. RMSD for residues comprising the flap.^[a]

Residue	Average RMSD [Å]	Standard Deviation [Å]	Maximum RMSD [Å]	Minimum RMSD [Å]
N76	3.0	0.6	5.7	1.2
Y77	1.7	0.4	3.3	0.4
V78	2.7	0.8	5.6	0.5
S79	2.4	0.7	5.1	0.6

[a] RMSD with respect to the reference crystal structure for residues comprising the flap region, averaged over the entire trajectory, with standard deviation as well as maximum and minimum values; RMSD measurements were carried out including all side chain atoms.

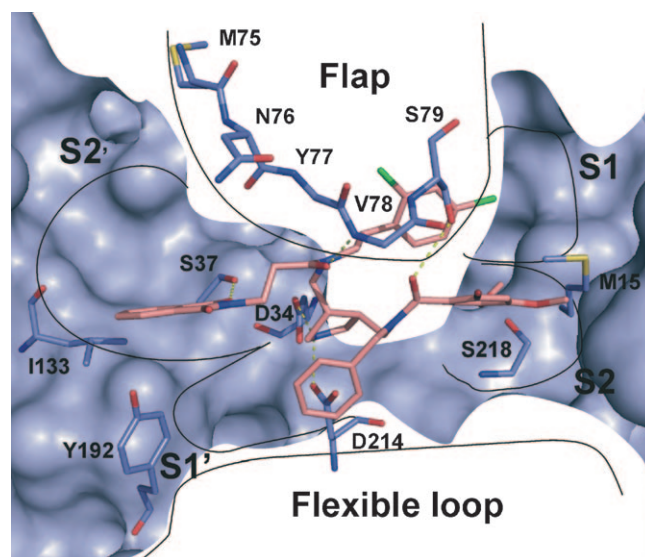


Figure 9. Manual placement of the pyrrolidine scaffold **3** (inhibitor **3.2**) in a MD-generated snapshot exhibiting an open conformation of the flap. After geometry minimization with MOLOC, hydrogen bonds to D34, D214, V78, S79, and S37 were formed (dashed yellow line).

optimized using MOLOC, assigning full flexibility of the ligand and keeping the protein rigid. The phthalimide substituent was placed into the S2' pocket, suggesting hydrogen bond formation to S37. The benzyl moiety is placed into the S1' pocket, the 2-bromo-4,5-dimethoxyphenyl substituent into the S2 pocket, and the 2,4-dichlorophenyl ring occupies the S1 pocket. For **3.1** an equivalent binding mode could be generated, pointing its unsubstituted phenyl substituent into the S2' pocket.

Relevance and implications for inhibitor design

Plms are difficult targets for structure-based ligand design due to their high structural flexibility. As a consequence, routine drug-design protocols based on a single rigid protein conformer of the binding site are insufficient to successfully predict reasonable binding modes. It is likely that the originally selected binding pocket would only be suitable to accommodate a limited fraction of the ligands tested by virtual screening. As long as

full flexibility of the protein structure cannot be handled simultaneously or in an adaptive manner during docking in the virtual screening campaign, the currently favored strategy we propose is to use a limited set of representative protein conformers to capture all possible alternatives in a comprehensive way. This set of parent conformers may be derived from either multiple experimental crystal structures or individual frames from MD simulations.

With respect to crystal structures, the available data undoubtedly display relevant conformations. In our design they served as a set of reference points generating reasonable binding modes for derivatives with **1** and **2** as core structures. However, because the presently determined crystal structures represent only three major distinct conformational states, it seems unlikely that they sufficiently cover the broad spectrum of potentially binding-competent protein conformers. This fact became evident for inhibitors with **3** as the scaffold.

In this study, highly flexible residues could be identified by MD simulation through analysis of residue mobility, and distinct conformers were identified. Based on the observed conformational opening of the flap during the MD simulation, a putative binding mode for the 3,4-bis(aminomethylene)pyrrolidine derivatives (**3.1** and **3.2**) was suggested. In general, the flexibility of the flap residues indicates that different linker lengths are well tolerated for inhibitors that are designed to directly address both the aspartates of the catalytic dyad and the flap residues. Furthermore, simulations of the uncomplexed state helped to understand surprising findings in two cases.^[36,45] The flexibility of M15 is responsible for the conformational opening of the S1 pocket. Therefore, elongated P1 substituents might be suitable to increase ligand affinity. The opening of the S2' pocket could be observed, allowing to accommodate bulky ligand side chains. This hypothesis is supported by the potent inhibitor **1.7** equipped with a bulky 1-naphthyl substituent directed into the S2' pocket. Hence, new ligands designed to explore the available space and properties of the S2' pocket in greater detail could possibly lead to more potent inhibitors.

Conclusions

In summary, we have discovered novel nonpeptidic inhibitors of Plm II and IV, featuring a pyrrolidine scaffold as core element. These compounds, originally designed for HIV-1 protease, show activity in the nanomolar range. Plausible binding modes could be suggested for the pyrrolidine-3,4-diester derivatives **1.1**–**1.7** and the 3,4-diaminopyrrolidine **2**, based on the Plm crystal structure (PDB ID: 1LEE) as a starting point. Putative binding modes for Plm II are in agreement with structure–activity relationships. Unfortunately, with the available crystallographic information it was not possible to generate a reasonable binding mode for the 3,4-bis(aminomethylene)pyrrolidine derivatives **3.1** and **3.2**. None of the three major binding-site conformers observed in the presently available crystal structures allow accommodation of the ligands. However, the structural studies indicate that Plm II is a highly flexible protein. To tackle this problem in greater detail, a MD simulation of the

uncomplexed state was carried out, and transitions along the trajectory were monitored. Supported by the MD simulation, a putative binding mode for the inhibitors with a 3,4-bis(aminomethylene)pyrrolidine scaffold **3** could be suggested. This provides further insight into binding pocket adaptations that possibly have implications for Plm II inhibitor design. In particular, the observed opening of the S1 and S2' pockets suggests the design of inhibitors with extended P1 and P2' residues. Furthermore, the search for new core scaffolds with different linker lengths can be of interest based on the observed flap flexibility.

Experimental Section

Assays and K_i determinations

The substrate used for the Plm II assay (Bachem) is a synthetic peptide [Abz-Thr-Ile-Nle-(*p*-nitro-Phe)-Gln-Arg-NH₂]. The Michaelis–Menten constant (K_M) for Plm II is 63 μM . The assays were performed with a Tecan Spectra Fluor spectrometer at excitation wavelength 337 nm and emission wavelength 414 nm. A volume of 180 μL assay buffer (0.1 M acetic acid/sodium acetate pH 4.5, 20 μM substrate, 2% DMSO) was added to 96-well plates. For the assay 18 μL of enzyme solution (0.1 M acetic acid/sodium acetate buffer, pH 4.5) were mixed with 2 μL inhibitor solution (dissolved in DMSO). After incubation for 5 min the enzyme–inhibitor solution was added to the 180 μL substrate solution (final enzyme concentration 1 nM). Substrate hydrolysis was recorded as an increase in fluorescence intensity over a period of 3 min.

IC_{50} values were converted into K_i values by applying the following equation:

$$K_i = [\text{IC}_{50} - (E_t/2)][1 + (S/K_M)]^{-1}$$

in which E_t is the total enzyme concentration (1 nM), K_M is the Michaelis–Menten constant (63 μM), and S is the substrate concentration (18 μM). Plm IV activity assays were performed similarly as described for Plm II. The enzyme concentration was 10 nM, $K_M = 28 \mu\text{M}$, and $S = 18 \mu\text{M}$. Cathepsin D activity assays were essentially performed as described for Plm II. The enzyme concentration was 1 nM, $K_M = 16 \mu\text{M}$, and $S = 9 \mu\text{M}$.

MD simulations

The MD simulation and all setup steps were performed as previously described^[36,45] using the Amber 8.0 suite of programs^[46] and the Amber 1999 force field. The plasmepsin structure (PDB ID: 1LEE) was used as starting point. After removal of the ligand and all crystallographic water molecules, hydrogens were added with PROTONATE. Protonation states were estimated with Poisson–Boltzmann calculations for all histidines and the aspartates of the catalytic dyad (D34 and D214) at pH 5: Both catalytic aspartates were assumed to be deprotonated, and all histidines were set to the protonated form. Subsequently, 200 steps of minimization were applied to the protein using a generalized Born solvation model. After addition of sodium counterions to ensure neutrality, the system was solvated in a box containing ~10 300 TIP3P water molecules.^[47] The solvated system was subjected to 200 steps of minimization.

The MD simulation was then started by heating the solvent to 300 K over a period of 20 ps and cooling to 100 K over a period of

5 ps, keeping the protein fixed. After this, the entire system was gradually brought to 300 K over a period of 25 ps. The simulation was carried out for 10 ns under constant temperature and pressure (NPT) applying periodic boundary conditions. A time step of 2 fs and PME (Particle–Mesh–Ewald)^[48] for evaluating the electrostatic interactions were used. Energy data were saved every 20 fs, and protein coordinates every 0.5 ps. CARNAL was used for further analysis of the trajectory, and VMD 1.8.2 for visualization.

The C^α atom RMSD with respect to the reference crystal structure was 2.1 ± 0.3 Å averaged over the trajectory, indicating a high stability of the overall fold (Figure 10). Considering all atoms, the trajectory-averaged RMSD value is 2.7 ± 0.3 Å, indicating more pronounced motions once the side chains are included in the analysis.

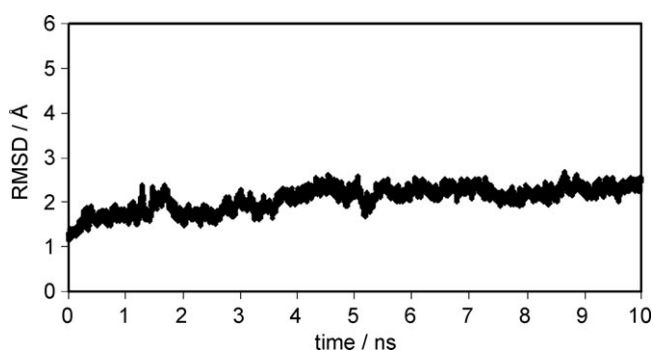


Figure 10. C^α atom RMSD in the MD simulation of Plm II.

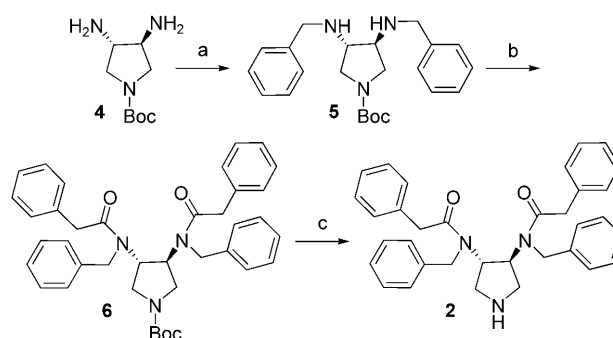
Synthesis

General: Reported yields refer to the analytically pure product obtained by column chromatography. All proton and carbon NMR spectra were recorded on a Jeol Eclipse+ spectrometer (¹H and ¹³C NMR: 400 or 500 MHz as indicated). ¹H NMR spectra were referenced to CDCl₃ (δ = 7.26 ppm) or [D₆]DMSO (δ = 2.50 ppm). ¹³C NMR spectra were referenced to CDCl₃ (δ = 77.16 ppm) or [D₆]DMSO (δ = 39.52 ppm). Chemical shift values (δ) are given in ppm and coupling constants (*J*) are given in Hz. Abbreviations: br = broad, ps = pseudo, s = singlet, d = doublet, t = triplet, q = quartet, smul = symmetric multiplet, m = multiplet. Mass spectra were obtained from a double focusing sector field Micromass VG-Autospec spectrometer. Combustion analyses were determined on a Vario Micro Cube by Elementar Analysen GmbH. Melting points were determined using a Leitz HM-Lux apparatus and are uncorrected. Flash chromatography (FC) was performed using silica gel 60 (0.04–0.063 mm) purchased from Macherey & Nagel. Solvents and reagents that are commercially available were used without further purification. All moisture-sensitive reactions were carried out using oven-dried glassware under a positive stream of argon.

Bis-benzylated pyrrolidine 5: Powdered molecular sieves (4 Å, 0.65 g) and benzaldehyde (0.79 mL, 7.8 mmol) were added to a solution of *tert*-butyl-(3*S*,4*S*)-3,4-diaminopyrrolidine-1-carboxylate^[49] (0.52 g, 2.6 mmol) in dry MeOH at room temperature. The suspension was stirred for 1 h under Ar. Subsequently, NaBH₄ (0.40 g, 10.4 mmol) was added portionwise at 0 °C. After stirring for 1 h at 0 °C, EtOAc (15 mL) and a saturated solution of NaHCO₃ (20 mL) were added. The suspension was filtered, and the filtrate was extracted with EtOAc (3 × 20 mL), dried over MgSO₄, filtered, and concentrated under reduced pressure. Purification via FC (hexanes/

EtOAc 3:7) yielded 0.58 g (59%) of the bis-benzylated pyrrolidine **5** as a pale-yellow oil: ¹H NMR (400 MHz, CDCl₃, 21.0 °C), rotamers: δ = 7.36–7.22 (m, 10H), 3.87–3.58 (m, 6H), 3.14–3.00 (m, 4H), 1.51 (s, 2H), 1.46 ppm (s, 9H); ¹³C NMR (100 MHz, CDCl₃, 21.0 °C), rotamers: δ = 28.6, 50.4, 51.0, 52.4, 61.2, 62.1, 79.4, 127.2, 128.2, 128.6, 140.1, 154.7 ppm; MS (ESI) *m/z* (%): 785 (24) [2*M*+Na]⁺, 763 (45) [2*M*+H]⁺, 382 (100) [*M*+H]⁺; HRMS-ESI *m/z* [*M*+H]⁺ calcd for C₂₃H₃₂N₃O₂: 382.2495, found: 382.2507; Anal. calcd for C₂₃H₃₁N₃O₂·0.5 H₂O: C 70.74, H 8.26, N 10.76, found: C 70.71, H 8.04, N 10.60.

Bis-amide 6: Bis-benzylated pyrrolidine **5** (0.33 g, 0.86 mmol), 2-phenylacetic acid (0.29 g, 2.15 mmol), and 1-hydroxybenzotriazole (0.29 g, 2.15 mmol) were dissolved in DMF (5 mL) and cooled to 0 °C. Et₃N (0.45 mL, 3.23 mmol) was added, and the solution was stirred at 0 °C for 5 min. Subsequently, 1-ethyl-3-(3'-dimethylamino-propyl)carbodiimide hydrochloride (0.41 g, 2.15 mmol) was added, and the mixture was stirred at 0 °C for 10 min. After allowing the reaction mixture to reach room temperature, stirring was continued for 13 h. The reaction was quenched by the addition of H₂O (10 mL), followed by EtOAc (10 mL). The aqueous layer was extracted with EtOAc (3 × 10 mL). The combined organic layers were washed with brine (2 × 10 mL), dried over MgSO₄, filtered, and the solvent was removed under reduced pressure. Purification via FC (hexanes/EtOAc 7:3) yielded 0.47 g (89%) of the bis-amide **6** as colorless crystals: mp: 78 °C; ¹H NMR (500 MHz, [D₆]DMSO, 100 °C), rotamers: δ = 7.39–7.11 (m, 20H), 4.92 (brs 2H), 4.48 (psd, 4H), 3.74–3.53 (m, 4H), 3.30 (s, 2H), 3.16 (brs, 2H), 1.32 ppm (s, 9H); ¹³C NMR (125.7 MHz, [D₆]DMSO, 100 °C), rotamers: δ = 27.4, 27.5, 27.6, 27.7, 45.0, 49.9, 56.6, 78.1, 125.9, 126.5, 127.6, 127.7, 127.9, 128.6, 134.9, 137.6, 152.8, 171.1 ppm; MS (ESI) *m/z* (%): 1257 (100) [2*M*+Na]⁺, 640 (63) [*M*+Na]⁺, 618 (12) [*M*+H]⁺; HRMS-ESI *m/z* [*M*+Na]⁺ calcd for C₃₉H₄₃N₃O₄Na: 640.3151, found: 640.3157; Anal. calcd for C₃₉H₄₃N₃O₄·0.5 H₂O: C 74.73, H 7.08, N 6.70, found: C 74.95, H 7.08, N 6.81.



Scheme 1. Synthesis of inhibitor **2**. Reagents and conditions: a) MeOH, powdered molecular sieves (4 Å), benzaldehyde, NaBH₄, 2 h, 59%; b) 2-phenylacetic acid, 1-hydroxybenzotriazole, DMF, EDCI, 13 h, 89%; c) Et₂O, HCl in Et₂O, 24 h, 91%.

Pyrrolidine 2 (Scheme 1): HCl in Et₂O (5 mL, 2 M) was added to bis-amide **6** (0.11 g, 0.18 mmol) in dry Et₂O (5 mL) at room temperature, and the solution was stirred for 24 h under Ar. The solvent was subsequently removed under reduced pressure. Purification was carried out by FC (CH₂Cl₂/MeOH 9:1) to yield 0.17 g (91%) of pyrrolidine **2** as a pale-yellow powder: mp: 43 °C; ¹H NMR (500 MHz, [D₆]DMSO, 100 °C), rotamers: δ = 7.39–7.10 (m, 20H), 5.67 (s, 1H), 4.52 (psd 6H), 3.70–3.48 (m, 4H), 2.89 (brs, 2H), 2.74 ppm (brs, 2H); ¹³C NMR (125.7 MHz, [D₆]DMSO, 100 °C), rotam-

ers: $\delta = 39.9, 48.0, 50.3, 60.4, 125.8, 126.0, 126.5, 127.6, 127.9, 128.5, 135.0, 137.9, 170.8$ ppm; MS (ESI) m/z (%): 518 (100) $[M+H]^+$; HRMS-ESI m/z $[M+H]^+$ calcd for $C_{34}H_{36}N_3O_2$: 518.2808, found: 518.2838; Anal. calcd for $C_{34}H_{35}N_3O_2 \cdot 0.5H_2O$: C 77.54, H 6.89, N 7.98, found: C 76.99, H 6.94, N 7.96.

Acknowledgements

We gratefully acknowledge financial support of our research by the DFG-Graduiertenkolleg GRK 541 "Proteinfunktion auf atomarer Ebene" (T.L.), the joint DFG research project KL1204/5-3 and DI827/3-2, and the Studienstiftung des deutschen Volkes (N.K.). The authors are grateful to Serghei Glinca for technical help. The clone of the protease was kindly provided by Prof. Dr. Daniel E. Goldberg, Department of Molecular Microbiology, Washington University School of Medicine, St. Louis, MO (USA).

Keywords: induced-fit adaptations · ligand design · molecular dynamics · plasmepsins · pyrrolidine derivatives

- [1] World Health Organization (WHO), *The World Health Report 2004*, <http://www.who.int/whr/2004/en/> (accessed January 4, 2010).
- [2] G. E. Linares, J. B. Rodriguez, *Curr. Med. Chem.* **2007**, *14*, 289.
- [3] *Antimalarial Chemotherapy: Mechanisms of Action, Resistance, and New Directions in Drug Discovery* (Ed.: P. J. Rosenthal), Humana Press, Totowa, 2001.
- [4] I. Y. Gluzman, S. E. Francis, A. Oksman, C. E. Smith, K. L. Duffin, D. E. Goldberg, *J. Clin. Invest.* **1994**, *93*, 1602.
- [5] K. K. Eggleston, K. L. Duffin, D. E. Goldberg, *J. Biol. Chem.* **1999**, *274*, 32411.
- [6] J. A. Bonilla, T. D. Bonilla, C. A. Yowell, H. Fujioka, J. B. Dame, *Mol. Microbiol.* **2007**, *65*, 64.
- [7] G. H. Coombs, D. E. Goldberg, M. Klemba, C. Berry, J. Kay, J. C. Mottram, *Trends Parasitol.* **2001**, *17*, 532.
- [8] S. E. Francis, I. Y. Gluzman, A. Oksman, A. Knickerbocker, R. Mueller, M. L. Bryant, D. R. Sherman, D. G. Russell, D. E. Goldberg, *EMBO J.* **1994**, *13*, 306.
- [9] R. P. Moon, L. Tyas, U. Certa, K. Rupp, D. Bur, C. Jacquet, H. Matile, H. Loetscher, F. Grueninger-Leitch, J. Kay, B. M. Dunn, C. Berry, R. G. Ridley, *Eur. J. Biochem.* **1997**, *244*, 552.
- [10] K. Ersmark, B. Samuelsson, A. Hallberg, *Med. Res. Rev.* **2006**, *26*, 626.
- [11] D. E. Goldberg, A. F. G. Slater, R. Beavis, B. Chait, A. Cerami, G. B. Henderson, *J. Exp. Med.* **1991**, *173*, 961.
- [12] J. B. Dame, G. R. Reddy, C. A. Yowell, B. M. Dunn, J. Kay, C. Berry, *Mol. Biochem. Parasitol.* **1994**, *64*, 177.
- [13] M. J. Humphreys, R. P. Moon, A. Klinder, S. D. Fowler, K. Rupp, D. Bur, R. G. Ridley, C. Berry, *FEBS Lett.* **1999**, *463*, 43.
- [14] A. L. Omara-Opyene, P. A. Moura, C. R. Sulsona, J. A. Bonilla, C. A. Yowell, H. Fujioka, D. A. Fidock, J. B. Dame, *J. Biol. Chem.* **2004**, *279*, 54088.
- [15] J. Liu, I. Y. Gluzman, M. E. Drew, D. E. Goldberg, *J. Biol. Chem.* **2004**, *280*, 1432.
- [16] E. Specker, J. Böttcher, H. Lilie, A. Heine, A. Schoop, G. Müller, N. Griebenow, G. Klebe, *Angew. Chem.* **2005**, *117*, 3200; *Angew. Chem. Int. Ed.* **2005**, *44*, 3140.
- [17] E. Specker, J. Böttcher, S. Brass, A. Heine, H. Lilie, A. Schoop, G. Müller, N. Griebenow, G. Klebe, *ChemMedChem* **2006**, *1*, 106.
- [18] J. Böttcher, A. Blum, S. Dörr, A. Heine, W. E. Diederich, G. Klebe, *ChemMedChem* **2008**, *3*, 1337.
- [19] A. Nezami, I. Luque, T. Kimura, Y. Kiso, E. Freire, *Biochemistry* **2002**, *41*, 2273.
- [20] K. Ersmark, I. Feierberg, S. Bjelic, J. Hultén, B. Samuelsson, J. Åqvist, A. Hallberg, *Bioorg. Med. Chem.* **2003**, *11*, 3723.
- [21] K. T. Andrews, D. P. Fairlie, P. K. Madala, J. Ray, D. M. Wyatt, P. M. Hilton, L. A. Melville, L. Beattie, D. L. Gardiner, R. C. Reid, M. J. Stoermer, T. Skinner-Adams, C. Berry, J. S. McCarthy, *Antimicrob. Agents Chemother.* **2006**, *50*, 639.
- [22] S. Bjelic, M. Nervall, H. Gutiérrez-de-Terán, K. Ersmark, A. Hallberg, J. Åqvist, *Cell. Mol. Life. Sci.* **2007**, *17*, 2285.
- [23] S. K. Pranav Kumar, V. M. Kulkarni, *Drug Des. Discovery* **2001**, *17*, 293.
- [24] K. Ersmark, M. Nervall, E. Hamelink, L. K. Janka, J. C. Clemente, B. M. Dunn, M. J. Blackman, B. Samuelsson, J. Åqvist, A. Hallberg, *J. Med. Chem.* **2005**, *48*, 6090.
- [25] H. Gutiérrez-de-Terán, M. Nervall, B. M. Dunn, J. C. Clemente, J. Åqvist, *FEBS Lett.* **2006**, *580*, 5910.
- [26] H. Gutiérrez-de-Terán, M. Nervall, K. Ersmark, P. Liu, L. K. Janka, B. Dunn, A. Hallberg, J. Åqvist, *Biochemistry* **2006**, *45*, 10529.
- [27] K. Ersmark, M. Nervall, H. Gutiérrez-de-Terán, E. Hamelink, L. K. Janka, J. C. Clemente, B. M. Dunn, A. Gogoll, B. Samuelsson, J. Åqvist, A. Hallberg, *Bioorg. Med. Chem.* **2006**, *14*, 2197.
- [28] K. Ersmark, I. Feierberg, S. Bjelic, E. Hamelink, F. Hackett, M. J. Blackman, J. Hultén, B. Samuelsson, J. Åqvist, A. Hallberg, *J. Med. Chem.* **2004**, *47*, 110.
- [29] R. Friedman, A. Caflich, *Proteins Struct. Funct. Bioinf.* **2008**, *73*, 814.
- [30] P. A. Valiente, P. R. Batista, A. Pupo, T. Pons, A. Valencia, P. G. Pascutti, *Proteins Struct. Funct. Bioinf.* **2008**, *73*, 440.
- [31] R. Friedman, A. Caflich, *ChemMedChem* **2009**, *4*, 1317.
- [32] I. D. Kuntz, K. Chen, K. A. Sharp, P. A. Kollman, *Proc. Natl. Acad. Sci. USA* **1999**, *96*, 9997.
- [33] A. L. Hopkins, C. R. Groom, A. Alex, *Drug Discovery Today* **2004**, *9*, 430.
- [34] C. H. Reynolds, S. D. Bembenek, B. A. Tounge, *Bioorg. Med. Chem. Lett.* **2007**, *17*, 4258.
- [35] C. H. Reynolds, B. A. Tounge, S. D. Bembenek, *J. Med. Chem.* **2008**, *51*, 2432.
- [36] T. Luksch, N.-S. Chan, S. Brass, C. A. Sotriffer, G. Klebe, W. E. Diederich, *ChemMedChem* **2008**, *3*, 1323.
- [37] A. Gustchina, I. T. Weber, *FEBS Lett.* **1990**, *269*, 269.
- [38] A. M. Silva, A. Y. Lee, S. V. Gulnik, P. Majer, J. Collins, T. N. Bhat, P. J. Collins, R. E. Cachau, K. E. Luker, I. Y. Gluzman, S. E. Francis, A. Oksman, D. E. Goldberg, J. W. Erickson, *Proc. Natl. Acad. Sci. USA* **1996**, *93*, 10034.
- [39] O. A. Asojo, E. Afonina, S. V. Gulnik, B. Yu, J. W. Erickson, R. Randa, D. Medjahed, A. M. Silva, *Acta Crystallogr. Sect. A* **2002**, *58*, 2001.
- [40] O. A. Asojo, S. V. Gulnik, E. Afonina, B. Yu, J. A. Ellman, T. S. Haque, A. M. Silva, *J. Mol. Biol.* **2003**, *327*, 173.
- [41] L. Prade, A. F. Jones, C. Boss, S. Richard-Bildstein, S. Meyer, C. Binkert, D. Bur, *J. Biol. Chem.* **2005**, *280*, 23837.
- [42] S. Cabani, G. Conti, L. Lepori, *Trans. Faraday Soc.* **1971**, *67*, 1933.
- [43] P. Czodrowski, C. A. Sotriffer, G. Klebe, *J. Chem. Inf. Comput. Sci.* **2007**, *47*, 1590.
- [44] P. R. Gerber, K. Müller, *J. Comput. Aided Mol. Des.* **1995**, *9*, 251.
- [45] S. Weik, T. Luksch, A. Evers, J. Böttcher, C. A. Sotriffer, A. Hasilik, H.-G. Löffler, G. Klebe, J. Rademann, *ChemMedChem* **2006**, *1*, 445.
- [46] D. A. Case, T. E. Cheatham, T. Darden, H. Gohlke, R. Luo, K. M. Merz, A. Onufriev, C. Simmerling, B. Wang, R. J. Woods, *J. Comput. Chem.* **2005**, *26*, 1668.
- [47] W. L. Jorgensen, J. Chandrasekhar, J. D. Madura, R. W. Impey, M. L. Klein, *J. Chem. Phys.* **1983**, *79*, 926.
- [48] T. Darden, D. York, L. Pedersen, *J. Chem. Phys.* **1993**, *98*, 10089.
- [49] A. Blum, J. Böttcher, A. Heine, G. Klebe, W. E. Diederich, *J. Med. Chem.* **2008**, *51*, 2078.

Received: November 1, 2009

Revised: December 18, 2009

Published online on January 28, 2010